Fiber-Coupled Single-Photon Detectors Based on NbN Superconducting Nanostructures for Practical Quantum Cryptography and Photon-Correlation Studies

Practical quantum cryptography (QC) systems require ultrafast and high-quantum-efficiency (QE) single-photon detectors (SPD's)[1] with precise timing characteristics[2] and sufficiently low dark counts. For fiber-optic QC systems, SPD's working at the standard near-infrared (NIR) telecommunication wavelengths, namely 1.3 μm and/or 1.55 μm, with counting rates well above 10 MHz are required. In this wavelength range, the most popular InGaAs avalanche photodiodes have limited applicability because of their very large dark counts and significant afterpulsing.

We have already reported on our development of novel superconducting SPD's (SSPD's) based on nanostructured NbN superconducting meanders maintained at temperatures far below the NbN critical temperature T_c.[3–5] The physics of the SSPD operation principle have been explained within a phenomenological, hot-spot formation photoresponse model.[6,7]

The purpose of this article is to present the design and performance of a system of two integrated single-photon detectors based on two fiber-coupled SSPD's. Our two-channel system is designed for implementation in the telecommunication wavelength QC as well as for antibunching-type correlation studies of NIR photons emitted by quantum dots. Contrary to previous designs of fiber-coupled superconducting photon detectors, which required either room-temperature[8] or cryogenic[9] fiber positioning and adjustment, we developed a permanent optical-fiber coupling, which allows multiple thermal cycling of our detectors, robust performance, and room-temperature–like operation.

Figure 106.44 presents schematics of a complete cryogenic construction of our detectors. The insert is placed and sealed inside a standard liquid helium transport dewar. Two NbN SSPD's are glued on the bottom flange insert, as shown in Fig. 106.44(a), with the photon input and electrical output provided via a single- or multimode fiber and a semirigid coaxial cable, respectively. The SSPD nanostructures under study were fabricated according to a technological procedure described in detail in Ref. 10. We used 10-μm × 10-μm^2 NbN superconducting meander-type structures with 4-nm-thick, 120-nm-wide stripes and a 0.6 filling factor (stripe width to stripe width plus separation ratio). The implemented devices were characterized by the critical current density of 2 to 6 MA/cm^2 at 4.2 K and $T_c \approx 10$ K.

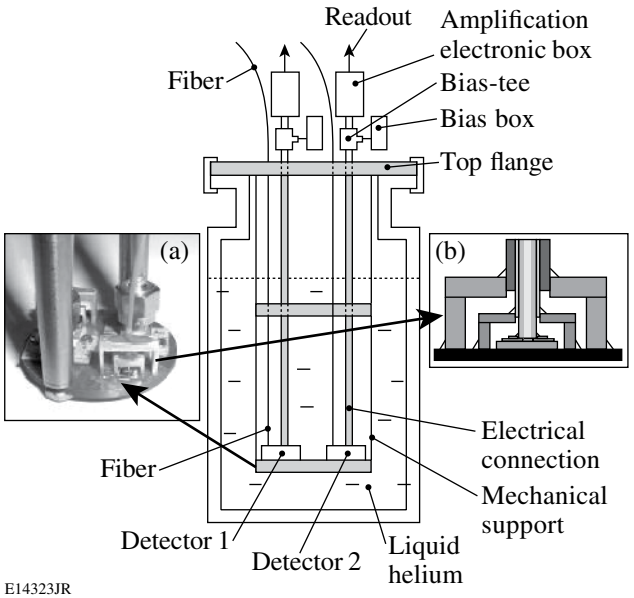

Figure 106.44
Schematic of the two-channel, single-photon detector operating in a helium transport dewar. (a) Cryogenic end plate with two detectors pigtailed to fibers and the electrical output SMA connectors and cryogenic semirigid cables. (b) Cross section of the fiber detector's mechanical holding structure with a fiber positioning photoresist ring.

For accurate coupling between the SSPD and the fiber, we used a specially designed micromechanical photoresist ring placed directly over the SSPD. The 30-μm-thick coupling rings were fabricated using a photolithography process and positioned over the NbN meander with an accuracy of ≤ 1 μm using the meander's original alignment marks.[11] A cross section of the photoresist ring and the fiber attachment mechanical support (two bridge-like aluminum holders) is presented in Fig. 106.44(b). Outside the dewar, as indicated in Fig. 106.44, each electrical channel was connected through a broadband

(0.08 to 26 GHz) bias-tee to a constant-voltage biasing circuit and a two-stage amplifier with 62-dB total gain and 0.05- to 4-GHz bandwidth. Optical fibers were equipped with standard FC-type connectors. The transport dewar, filled with 60 liters of helium, allowed for over 2 months of uninterrupted operation of our detectors.

We have so far fabricated a total of ten detectors (five integrated pairs) of which eight were coupled with single-mode fibers and two with multimode fibers. The basic qualification of the detector performance was the measurement of the system QE (SQE)[3,12,13] using highly attenuated, 40-ps-wide, 1540-nm-wavelength, 1-MHz repetition rate pulses from a semiconductor laser. The photon flux was precisely calibrated at the room-temperature fiber input (FC connector) and was the measure of the number of photons per optical pulse incident on the SSPD.

The detection probabilities (DP's) of several of our devices versus the number of photons per pulse delivered by the fiber to the NbN structure are presented in Fig. 106.45. The measurements were performed for the bias current $I_b = 0.95\ I_C$, where I_C is the SSPD critical current at 4.2 K. The behavior observed

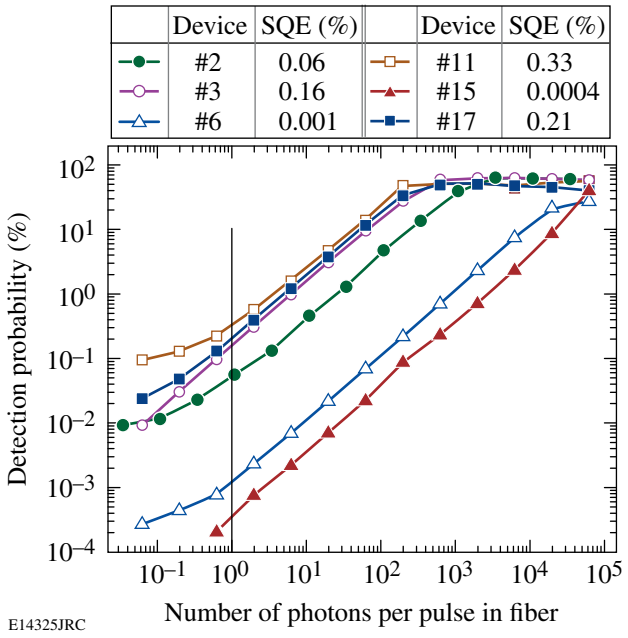

Figure 106.45
Photoresponse detection probability dependencies of the tested fiber-coupled NbN SSPD's on an average number of photons of the 1540-nm wavelength per pulse illuminating the detectors. For comparison purposes, the SQE value of the multimode fiber device #3 has been adjusted by taking into account the actual number of photons reaching the SSPD area. The thin vertical line indicates the 1 photon/pulse flux and corresponds to the SQE definition.

in Fig. 106.45 is in very good agreement with our previous observations.[3–6] At low-incident photon fluxes, our experimental data show the linear DP dependence, demonstrating the single-photon detection mechanism.[6] At high-light power levels, we observe DP saturation at the 100% level as virtually all laser pulses are counted. We define the SQE of our detectors by taking the DP value at the photon flux level corresponding to an average of one photon per pulse.

The SQE values for our best, average, and worst detectors are collected in Table 106.X with the device QE (DQE) values measured for the 1550-nm wavelength immediately after the SSPD fabrication. Taking the SQE/DQE ratio for each device, we have estimated and listed (see Table 106.X) the coupling factor K between the SSPD structure and the fiber. Simple calculations show (see Ref. 11) that the maximum $K \geq 0.9$ can be achieved when the fiber detectors' vertical separation is $<20\ \mu$m. However, K decreases rapidly with increasing horizontal misalignment and, for deviations $\geq 8\ \mu$m K, drops below 0.1. Table 106.X demonstrates that only device #11 exhibits a relatively large $K = 0.333$ factor while the "average" K is only 0.03, suggesting significant misalignment in the horizontal plane. Since the photoresist ring anchoring the fiber was positioned with 1-μm precision, we suspect that the observed low K values have their origin in an uncontrolled fiber tilting, resulting in an angled front surface of the fiber pigtailed to the detector. Thicker photoresist rings with tighter control of the inner circle diameter should significantly improve K.

Table 106.X: Device and system QE values for single-mode, 12-μm core diameter, fiber-coupled NbN SSPD detectors.

Detector #	DQE (%)	SQE (%)	Coupling factor K
11	1.0	0.33	0.333
2	2.1	0.06	0.029
17	6.4	0.21	0.033
6	2.0	0.001	0.0005
15	2.1	0.0004	0.0002

The reason for very low K values in devices #6 and #15 are apparently microcracks of the fiber core, which are likely to happen during the very first cooling cycle of the detector. The latter seems to be supported by the fact that in all our devices K remained unchanged after the initial one or two thermal cycles (300 K to 4.2 K and back) and the fatal detector failures were typically observed during/after the first cooldown. Postmortem mechanical inspection showed the fiber cracks in the damaged detectors.

The performance of detectors equipped with multimode (50-μm core diameter) fibers was not as good as expected (see, e.g., device #3 in Fig. 106.45) and the corresponding SQE and K values were rather low. The photon beam profile in the core of a multimode fiber has a Gaussian distribution; thus, even in case of optimum alignment, only ~10% of the power from the fiber reaches our 100 μm^2 SSPD. It is clear that larger area (e.g., 10×20 μm^2 or even 20×20 μm^2) SSPD's and fibers with reduced core diameters are needed to make the multimode fiber devices practical.

The dark count measurements performed on our detectors with the fiber room-temperature input blocked and biased at $I_b = 0.95\, I_C$ resulted in 2 (device #6) to 90 (device #11) counts per second, clearly depending on the detector's K factor. The observed dark counts are significantly higher than that measured in our earlier free-space NbN detectors.[3] The apparent reason is the 300-K thermal background radiation picked by the fiber's room-temperature end.

The SSPD's used to fabricate our fiber-coupled detectors were large-area meanders to maximize K. As recently documented,[14,15] such structures exhibit large kinetic inductance, which limits their photoresponse temporal characteristics. In our time-domain measurements, we used 5-GHz-bandwidth, single-shot and 50-GHz-bandwidth, sampling oscilloscopes for capturing transient waveforms and for jitter studies, respectively. Figure 106.46 shows a photoresponse signal (dotted line) of one of our detectors. The measured transient is characterized by a 250-ps rise time, 5-ns fall time, and a full width at half maximum (FWHM) equal to about 2.5 ns. We compared the measured pulse shape with numerical simulations (solid line) based on a model developed in Ref. 15 and confirmed that the kinetic inductance was responsible for a nanosecond-wide photoresponse of large-area SSPD's.

The experimental jitter profile (not shown) had a Gaussian shape and exhibited a FWHM of 35 to 37 ps for detectors with single-mode fibers. We note that the jitter measured in the fiber-coupled detectors is two times longer than the 18-ps value reported earlier for free-space–coupled SSPD's.[3] The large kinetic inductance of the SSPD's may contribute to the jitter increase, although we believe that the excess jitter is due to such extrinsic elements as the laser-diode jitter and relatively long (>1 m) fiber and electrical cables.

Finally, we used our integrated, two-detector system in cross-correlation–type experiments. A train of 500-fs-wide (stretched by the fiber) pulses from a Ti:sapphire laser with a 940-nm wavelength and an 82-MHz repetition rate was split by a 50/50 beam splitter and directed simultaneously to the two detectors. Next, the signal from each detector was sent to a discriminator and fed to a start/stop-type correlator. The detector with a low SQE of 0.005% worked as a start device, while our best (#11) detector provided the stop signal. The resulting experimental second-order correlation function is shown in Fig. 106.47. The correlation signal is very clean and exhibits a FWHM of 390 ps, which can be regarded as the

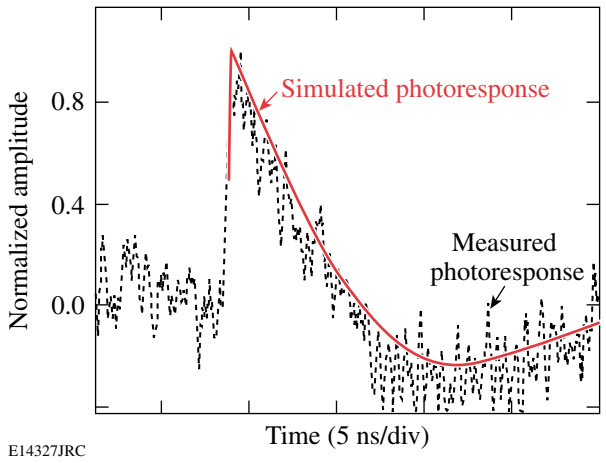

Figure 106.46
Time-resolved photoresponse of a fiber-coupled, 100-μm^2 area SSPD (dotted line) and the simulated signal (solid line) based on the calculated 420-nH value of the SSPD kinetic inductance and the 0.05- to 4-GHz bandwidth amplifier.

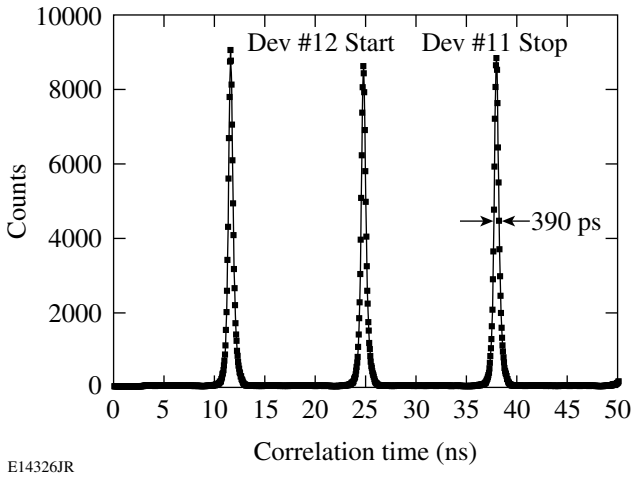

Figure 106.47
Experimental cross-correlation function of a pair of fiber-coupled detectors measured for 500-fs-wide incident optical pulses. The measured correlation FWHM is 390 ps.

figure of merit of the complete detection system (amplifiers, discriminator, correlator, cables, terminators, and detectors) since the incident optical pulses are negligibly short. We note that, despite a relatively long (few nanosecond in duration) response times of our detectors, the correlation pulses are subnanosecond. The latter, we believe, is due to the very low jitter and the short (250-ps) photoresponse rise time of the SSPD's and demonstrates the ability of our fiber-coupled detectors to successfully perform antibunching-type correlations observed in photons emitted by true single-photon sources such as single quantum dots.[16]

In conclusion, we have fabricated and tested fiber-based, single-photon detectors with a SQE of 0.3% at the 1550-nm telecommunication wavelength and fiber-coupling factor of up to 33%. The integrated two-detector arrangements can be placed inside a standard helium dewar and, from the operator's point of view, can be regarded as a room-temperature system. Our detectors are intended as practical devices for fiber-based QC systems since, despite their relatively low SQE, they are characterized by a counting rate above 200 MHz, jitter below 40 ps, and dark-count rates below 100 Hz. We have also demonstrated that the system cross-correlation time of two detectors counting femtosecond optical pulses is as low as 390 ps, making our fiber-coupled SSPD's very attractive for time-resolved, antibunching-type studies of single-photon sources. Our current research focuses on an improvement of the SQE and we expect to reach the 3% to 5% level because of the increase in DQE of our SSPD's and the achievement of reproducible K values of 30% or more. Very-large-area meander structures and devices coupled to quarter-wave resonators will be also implemented, especially in detectors with multimode fibers.

ACKNOWLEDGMENT

The authors would like to thank Dr. Marc Currie for his assistance in early time-resolved photoresponse measurements and Prof. Atac Imamoglu for his support. This work was supported by the Polish Ministry of Science under Project No. 3 T11B 052 26 (Warsaw), RFBR 03-02-17697 and INTAS 03-51-4145 grants (Moscow), CRDF grants RE2-2531-MO-03 (Moscow) and RE2-2529-MO-03 (Moscow and Rochester), and US AFOSR FA9550-04-1-0123 (Rochester). Additional support was provided by the MIT Lincoln Laboratory and BBN Technologies grants.

REFERENCES

1. J. C. Livas *et al*., in *Free-Space Laser Communication Technologies VII*, edited by G. S. Mecherle (SPIE, Bellingham, WA, 1995), Vol. 2381, pp. 38–47.
2. C. Kurtsiefer *et al*., in *Quantum Optics in Computing and Communications*, edited by S. Liu, G. Guo, H.-K. Lo, and N. Imoto (SPIE, Bellingham, WA, 2002), Vol. 4917, pp. 25–31.
3. A. Verevkin, A. Pearlman, W. Słysz, J. Zhang, M. Currie, A. Korneev, G. Chulkova, O. Okunev, P. Kouminov, K. Smirnov, B. Voronov, G. N. Gol'tsman, and R. Sobolewski, J. Mod. Opt. **51**, 1447 (2004).
4. A. Korneev, P. Kouminov, V. Matvienko, G. Chulkova, K. Smirnov, B. Voronov, G. N. Gol'tsman, M. Currie, W. Lo, K. Wilsher, J. Zhang, W. Słysz, A. Pearlman, A. Verevkin, and R. Sobolewski, Appl. Phys. Lett. **84**, 5338 (2004).
5. G. N. Gol'tsman, K. Smirnov, P. Kouminov, B. Voronov, N. Kaurova, V. Drakinsky, J. Zhang, A. Verevkin, and R. Sobolewski, IEEE Trans. Appl. Supercond. **13**, 192 (2003).
6. G. N. Gol'tsman, O. Okunev, G. Chulkova, A. Lipatov, A. Semenov, K. Smirnov, B. Voronov, A. Dzardanov, C. Williams, and R. Sobolewski, Appl. Phys. Lett. **79**, 705 (2001).
7. A. D. Semenov, G. N. Gol'tsman, and A. A. Korneev, Physica C **351**, 349 (2001).
8. A. J. Miller *et al*., Appl. Phys. Lett. **83**, 791 (2003).
9. J. Zhang, N. Boiadjieva, G. Chulkova, H. Deslandes, G. N. Gol'tsman, A. Korneev, P. Kouminov, M. Leibowitz, W. Lo, R. Malinsky, O. Okunev, A. Pearlman, W. Słysz, K. Smirnov, C. Tsao, A. Verevkin, B. Voronov, K. Wilsher, and R. Sobolewski, Electron. Lett. **39**, 1086 (2003).
10. G. N. Gol'tsman, A. Korneev, I. Rubtsova, I. Milostnaya, G. Chulkova, O. Minaeva, K. Smirnov, B. Voronov, W. Słysz, A. Pearlman, A. Verevkin, and R. Sobolewski, Phys. Stat. Sol. C **2**, 1480 (2005).
11. P. Grabiec, W. Słysz, M. Węgrzecki, J. Bar, W. Milczarek, G. N. Gol'tsman, A. Verevkin, and R. Sobolewski, Poland Patent No. P-367391 (patent pending, 2004).
12. A. Verevkin, J. Zhang, R. Sobolewski, A. Lipatov, O. Okunev, G. Chulkova, A. Korneev, K. Smirnov, G. N. Gol'tsman, and A. Semenov, Appl. Phys. Lett. **80**, 4687 (2002).
13. W. Słysz, M. Węgrzecki, J. Bar, P. Grabiec, M. Górska, C. Latta, V. Zwiller, A. Pearlman, A. Cross, A. Korneev, P. Kouminov, K. Smirnov, B. Voronov, G. Gol'tsman, A. Verevkin, M. Currie, and R. Sobolewski, in *Infrared Photoelectronics*, edited by A. Rogalski, E. L. Dereniak, and F. F. Sizov (SPIE, Bellingham, WA, 2005), Vol. 5957, pp. 310–319.
14. R. H. Hadfield *et al*., Appl. Phys. Lett. **87**, 203505 (2005).
15. A. J. Kerman *et al*., Appl. Phys. Lett. **88**, 111116 (2006).
16. V. Zwiller *et al*., Appl. Phys. Lett. **78**, 2476 (2001).